Research Square

Preprints are preliminary reports that have not undergone peer review.
They should not be considered conclusive, used to inform clinical practice,
or referenced by the media as validated information.

Simulation Study on Defeat Formation of a Novel Highly Integrated Die- Casting Process

Bingwei Wu
Nanjing University of Aeronautics and Astronautics
Bing Ye
Shanghai Jiao Tong University
Zhiguo Lin
Nanjing University of Aeronautics and Astronautics
Qiang Gao
Nanjing University of Aeronautics and Astronautics
Qigui Wang
General Motors
Wenying Yang
General Motors
Wenhao Pu
paulpu@nuaa.edu.cn

Nanjing University of Aeronautics and Astronautics

Research Article

Keywords: die casting, highly integrated die casting, porosity, simulation

Posted Date: July 24th, 2026

DOI: https://doi.org/10.21203/rs.3.rs-10128590/v1

License: This work is licensed under a Creative Commons Attribution 4.0 International License.
Read Full License

Additional Declarations: No competing interests reported.

Version of Record: A version of this preprint was published at International Journal of Metalcasting on October 17th, 2026. See the published version at https://doi.org/10.1007/s40962-026-02156-2.

Simulation Study on Defeat Formation of a Novel Highly Integrated Die-Casting Process

Bingwei Wu[a,b], Bing Ye[b]*, Zhiguo Lin[a], Qiang Gao[a], Qigui Wang[c], Wenying Yang[c], Wenhao Pu[a]*,.

[a] College of Energy and Power Engineering, Nanjing University of Aeronautics and Astronautics, Yu Dao Street, Nanjing 210016, China

[b] School of Materials Science and Engineering, Shanghai Jiao Tong University, 800 Dong Chuan Road, Shanghai 200240, China

[c] Global Product Group, General Motors, Warren, MI, USA

Abstract: High-pressure die casting (HPDC) is extensively utilized in the automotive industry for efficiently manufacturing complex components, but it inherently suffers from significant porosity defects that deteriorate the subsequent mechanical properties of the castings. To solve the question, the highly integrated die casting (HIDC) process was developed and tested to significantly suppress porosity defects by our group. However, the mechanism of defect formation and the evolution law of flow and solidification of the HIDC process have not been fully elucidated. A refined three-dimensional model with dynamic mesh was developed to simulate the entire transient HIDC process of ADC12 aluminum alloy, encompassing the stages of low-pressure filling, depressurization, high-pressure injection, and solidification. Based on experimental data, the inlet velocity curve and piston position curve were incorporated as initial conditions, and the effect of liquid fraction on the wall heat transfer coefficient was taken into account. The simulation results agree well with the experimental data in terms of porosity area and defect distributions. The evolution of defect formation and solidification fraction in the HIDC Process were demonstrated. And effect of filling percentage and slow injection speed were discussed. It was found that a filling rate of 60% is the optimal value for balancing gas inclusions and stratified solidification defects, which is in good agreement with the experimental results. When the slow injection speeds increased from 0.09 m/s to 0.16 m/s, gas entrapment caused by melt backflow was mitigated, and the predicted porosity of the castings decrease from 7.2% to 0.29%.

Keywords: die casting, highly integrated die casting, porosity, simulation

1. Introduction

Against the backdrop of increasingly prominent environmental issues, vehicle light weighting is recognized as an effective strategy to address greenhouse gas emissions[1, 2].High-pressure die casting (HPDC) was widely used in the automotive industry to

*Corresponding author at: School of Materials Science and Engineering, Shanghai Jiao Tong University, 800 Dong Chuan Road, Shanghai 200240, China. Tel.: +86 21 54742715; Fax: +86 21 34202794.

E-mail address: bingye@sjtu.edu.cn (B. Ye), paulpu@nuaa.edu.cn (W. Pu)

manufacture components requiring high dimensional accuracy and low surface roughness, owing to its high productivity and cost-effective mass production capability [3, 4]. It was also capable of producing complex thin-walled components efficiently. However, the process typically resulted in significant porosity defects, which reduced mechanical properties and limited the applicability of subsequent heat treatment [5, 6]. Researchers have developed vacuum-assisted die casting[7, 8], super vacuum die casting[9, 10] and semi-solid metal die casting[11, 12] based on improvements to the HPDC process. The HIDC process also represents an improvement over the conventional HPDC process, as it significantly reduces gas porosity defects while maintaining relatively lower equipment and maintenance costs. Although HIDC effectively mitigated porosity issues in conventional die casting, the underlying mechanisms governing defect formation had not been fully clarified.

The modified HPDC process significantly enhances casting quality[13, 14]. Bai fabricated a high-strength $Al_{80}Si_8Mg_4Cu_4Zn_4$ alloy via vacuum-assisted die casting. After a solution treatment at 450 °C, the alloy achieved a yield strength of 566 ± 8 MPa[15]. Zheng reports that a three-stage ultra-vacuum HPDC process achieves a minimum cavity vacuum of 10 mbar, increasing the yield strength, tensile strength, and ductility by 3.65%, 3.55%, and 7.41%, respectively, while refining the microstructure and transforming the fracture mode to ductile-brittle mixed[16]. Kumar et al. investigated the filling behavior of semi-solid Al–10.5Si–1.7Cu alloy slurry during the rheo-pressure die casting process through combined simulation and experimental studies. It was found that a lower piston speed significantly reduces porosity defects by minimizing air entrapment in the overflow region[17]. Arcaleni characterized the microstructure of primary and recycled AlSi7Mg alloys processed by thixo-casting, demonstrating that high iron content in recycled alloys degrades the microstructure and Rheo-cast Quality Index, while low-iron recycled material performs comparably to the primary alloy[18]. Nevertheless, the adoption of such techniques entails increased equipment costs and operational complexity, which may limit their practical implementation in high-volume production scenarios[19].

Numerical simulation of the casting process had been widely applied by researchers, which provided a solid technical foundation for this study [20, 21]. Mahmoud employed FLOW-3D CAST to simulate the high-pressure die casting of a brass lock plate. The results showed that the simulation effectively predicted the locations of porosity caused by gas entrapment and shrinkage, which were consistent with the actual casting defects, thereby demonstrating the practical value of numerical simulation in process optimization and defect reduction [22]. Dou simulated the entire HPDC process of aluminum alloy specimens and analyzed the flow, solidification, and defect formation. They found a potential correlation between the turbulence level during injection and the reduction in elongation of the specimens. The simulation results were generally in good agreement with experimental data in terms of temperature distribution, solid fraction, and porosity prediction [23]. Wang investigated the effects of process parameters on mold filling and feeding capability through orthogonal experiments and numerical simulations. The results indicated that the piston velocity during the fast injection stage had the most significant influence. They also proposed an optimized range of process parameters and pointed out that premature solidification at the ingate weakened the pressure-holding effect [24].

Therefore, this study aims to clarify the defect formation and suppression mechanisms in the highly integrated die casting process through systematic numerical simulation. The research object is an ADC12 aluminum alloy casting produced by the HIDC process, which integrates low-pressure stable filling and high-pressure injection. A refined three-dimensional transient simulation model is established using to reproduce the complete process, including low-pressure melt feeding, shot-sleeve flow evolution, piston-driven mold filling, gas evacuation, heat transfer, and solidification. The innovation of this work lies in that, the present model considers the actual transient inflow and flow oscillation of the molten alloy before mold filling, instead of assuming a static and isothermal initial melt in the shot sleeve as commonly adopted in conventional die-casting simulations. Based on this model, the effects of filling percentage and slow injection speed on gas entrapment, stratified solidification, temperature evolution, and solidification sequence are investigated. The accuracy of the

model is validated by comparing the simulation results with X-ray images, aiming to provide guidance for parameter optimization and defect prediction in the HIDC process.

2. Highly integrated die casting

As shown in Fig.1, the HIDC experimental system consists of a thermal insulation device, a heating sleeve, a riser tube, a sealed crucible, and a die-casting machine, with the crucible being heated and insulated in an electric furnace. Under the action of compressed air, the molten alloy rises through the riser tube into the shot sleeve, and a piston drives the molten alloy to fill the mold cavity. The molten alloy solidifies under high pressure, resulting in a casting with a dense microstructure and low porosity defects. The photo of the HIDC system is shown in Fig.2.

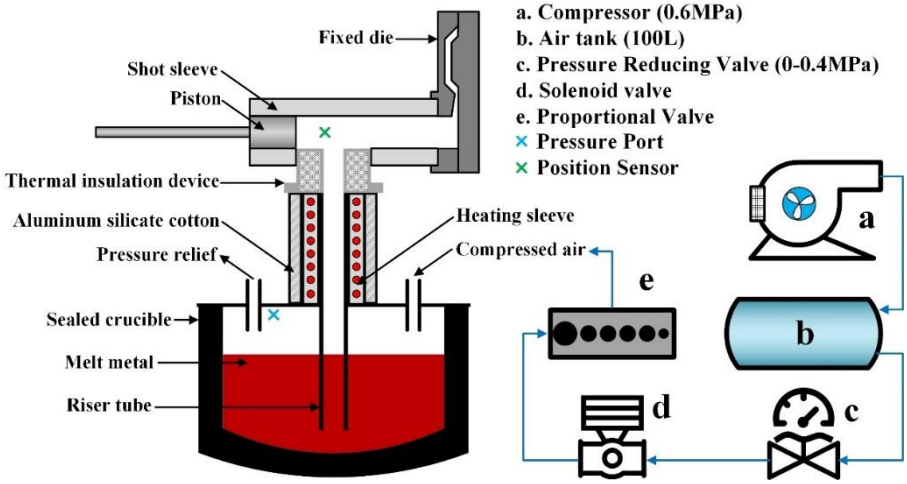


Fig.1 Highly integrated die casting system

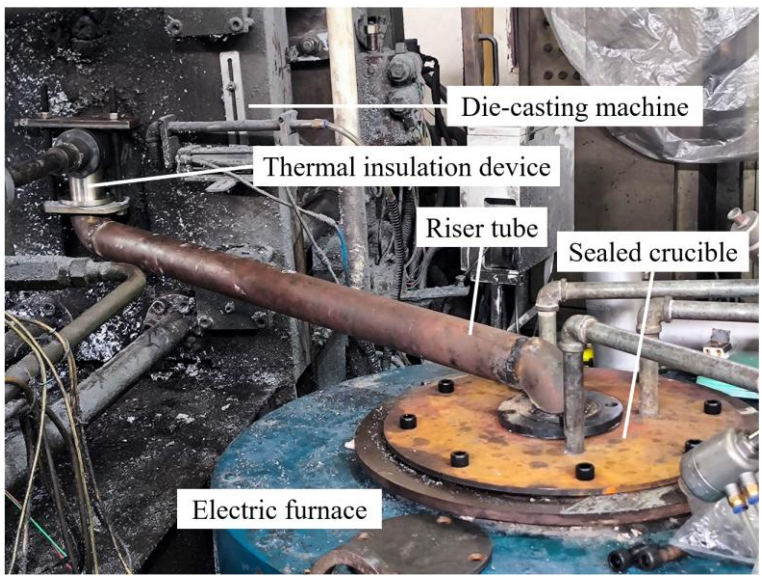


Fig.2 Photograph of the HIDC system

The HIDC process integrates low-pressure stable filling with high-pressure rapid injection, which effectively suppresses gas entrapment during mold filling. Fig.3 demonstrated the significant advantage of the HIDC process in reducing porosity defects in castings. By combining low-pressure stable filling with high-speed high-pressure injection, the HIDC process effectively reduced gas entrapment at the source during mold filling.

Experimental results showed that, compared with the conventional high-pressure die casting process, the HIDC process reduced the volumetric porosity of ADC12 aluminum alloy castings by 93.4%. In addition, the pores became finer and more uniformly distributed, which significantly improved the density and mechanical properties of the castings.

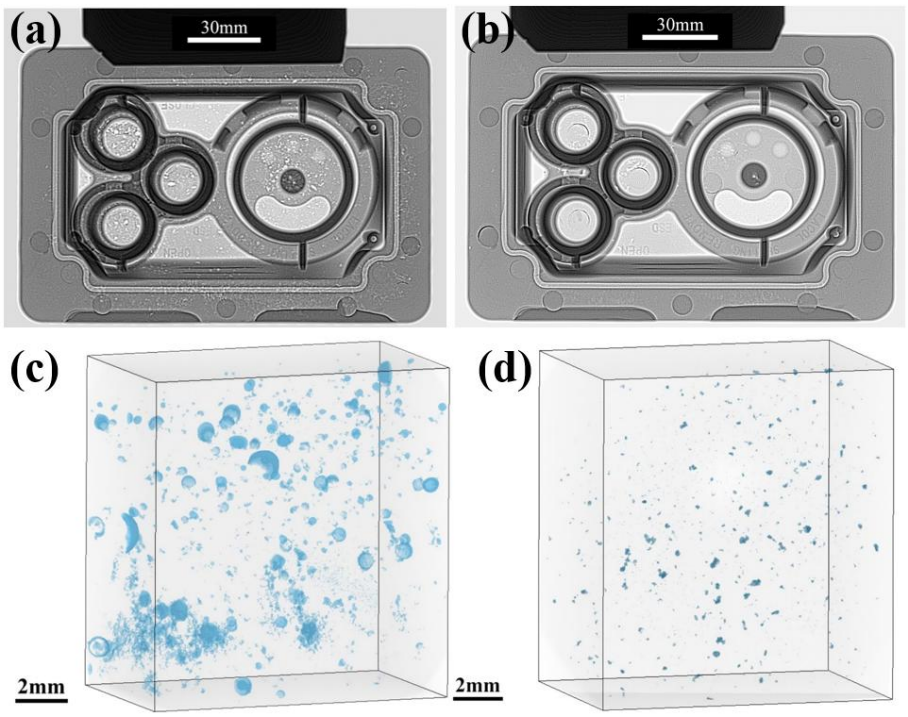


Fig.3 Effect of casting process on casting porosity: (a) 2D X-ray of HPDC; (b) 2D X-ray of HIDC; (c) X-ray CT of HPDC; (d) X-ray CT of HIDC

3. Simulation method of highly integrated die casting

3.1 Physical model

In this study, the turbulent model with k-ε equations is used to solve mass, momentum and energy conservation equations. The volume function method is normally applied to track the changing volume function of fluid surface.

Mass conservation:

$$\frac{d\rho}{dt}+\rho\left(\frac{\partial u}{\partial x}+\frac{\partial v}{\partial y}+\frac{\partial w}{\partial z}\right)=0 \quad (1)$$

Navier-Stokes equation:

$$\rho\left(\frac{\partial u}{\partial t}+u\frac{\partial u}{\partial x}+v\frac{\partial u}{\partial y}+w\frac{\partial u}{\partial z}\right)=-\frac{\partial p}{\partial x}+\rho g_x+\mu\nabla^2 u$$

$$\rho\left(\frac{\partial v}{\partial t}+u\frac{\partial v}{\partial x}+v\frac{\partial v}{\partial y}+w\frac{\partial v}{\partial z}\right)=-\frac{\partial p}{\partial x}+\rho g_y+\mu\nabla^2 v \quad (2)$$

$$\rho\left(\frac{\partial w}{\partial t}+u\frac{\partial w}{\partial x}+v\frac{\partial w}{\partial y}+w\frac{\partial w}{\partial z}\right)=-\frac{\partial p}{\partial x}+\rho g_z+\mu\nabla^2 w$$

Energy conservation:

$$\frac{\partial\left(\rho c_p T\right)}{\partial t}+\frac{\partial\left(\rho c_p u T\right)}{\partial x}+\frac{\partial\left(\rho c_p v T\right)}{\partial y}+\frac{\partial\left(\rho c_p w T\right)}{\partial z}=\frac{\partial\left(k\frac{\partial T}{\partial x}\right)}{\partial x}+\frac{\partial\left(k\frac{\partial T}{\partial y}\right)}{\partial y}+\frac{\partial\left(k\frac{\partial T}{\partial z}\right)}{\partial z}+S \quad (3)$$

The volume function:

$$\frac{\partial F}{\partial t}+\frac{\partial Fu}{\partial x}+\frac{\partial Fv}{\partial y}+\frac{\partial Fw}{\partial z}=0 \quad (4)$$

Where ∇ is the Laplace operator; ρ is the density; P is the pressure; T is the temperature; μ is the kinematic viscosity; c_p is the specific heat capacity at constant pressure; F is volume function, and$0 \leq F \leq 1$. In this study, a simplified Two-Phase VOF model has been implemented. It is assumed that the liquid and gas phases at a given node are assumed to have the same velocity, temperature and pressure. The properties such as density and viscosity are computed as volume fraction weighted average of the properties of the individual gas and liquid phases.

3.2 Numerical simulation conditions

In this study, the ProCAST software was used to simulate the entire HIDC process [25]. A simplified three-dimensional geometric model of the highly integrated die casting system was constructed using NX 12.0, as shown in Fig.4. The model consisted of the mold, fluid domain, shot sleeve, and piston. During the simulation, the molten

alloy entered the fluid domain through a mass flow inlet. The inlet velocity–time curve of the molten alloy was obtained from the numerical simulation of the low-pressure filling process. At a specified time, the piston moved leftward to gradually block the inlet. Once the inlet was completely blocked, the inlet velocity became zero, and no additional molten alloy entered the fluid domain. The piston then continued to move forward, pushing the molten alloy to fill the entire fluid domain. Meanwhile, the air inside the cavity was discharged through the exhaust ports. During the filling and solidification processes, the molten alloy transferred its sensible and latent heat to the mold, shot sleeve, and piston through convective heat transfer. Subsequently, the mold, shot sleeve, and piston dissipated heat to the surrounding air via natural convection.

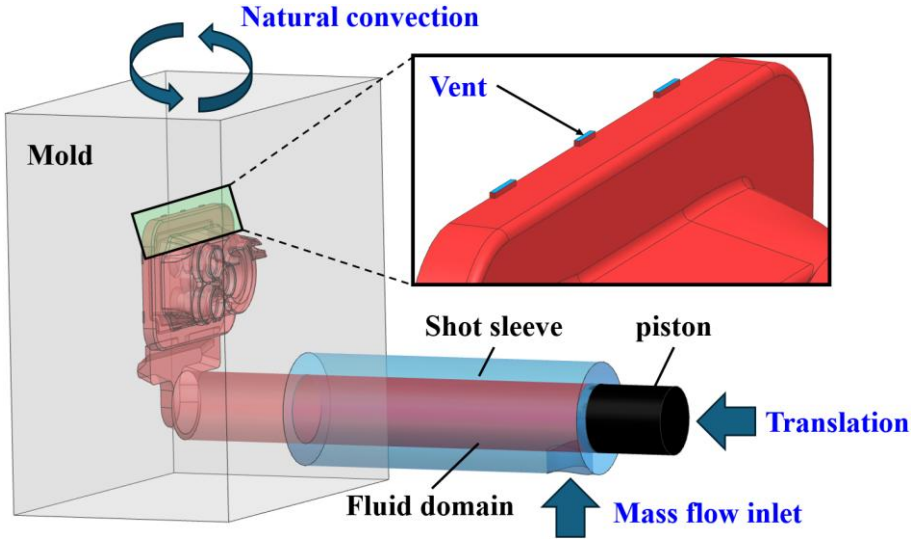


Fig.4 HIDC process: geometric model and boundary conditions

The same material as used in the experiments was adopted in the simulation, namely ADC12 aluminum alloy. Its chemical composition is listed in Table 1. The mold and shot sleeve materials were defined as H13 steel, which exhibits excellent thermal resistance and mechanical properties at elevated temperature and is widely used in aluminum alloy die casting molds. During the casting process, the thermophysical properties of the molten metal, including density, thermal conductivity, enthalpy, and solid fraction, varied significantly with temperature. Similarly, the thermal conductivity and enthalpy of H13 steel also changed with temperature. These temperature-dependent properties of ADC12 alloy and H13 steel were calculated using the Scheil model. The

variation of thermophysical properties of ADC12 alloy with temperature is shown in Fig.5.

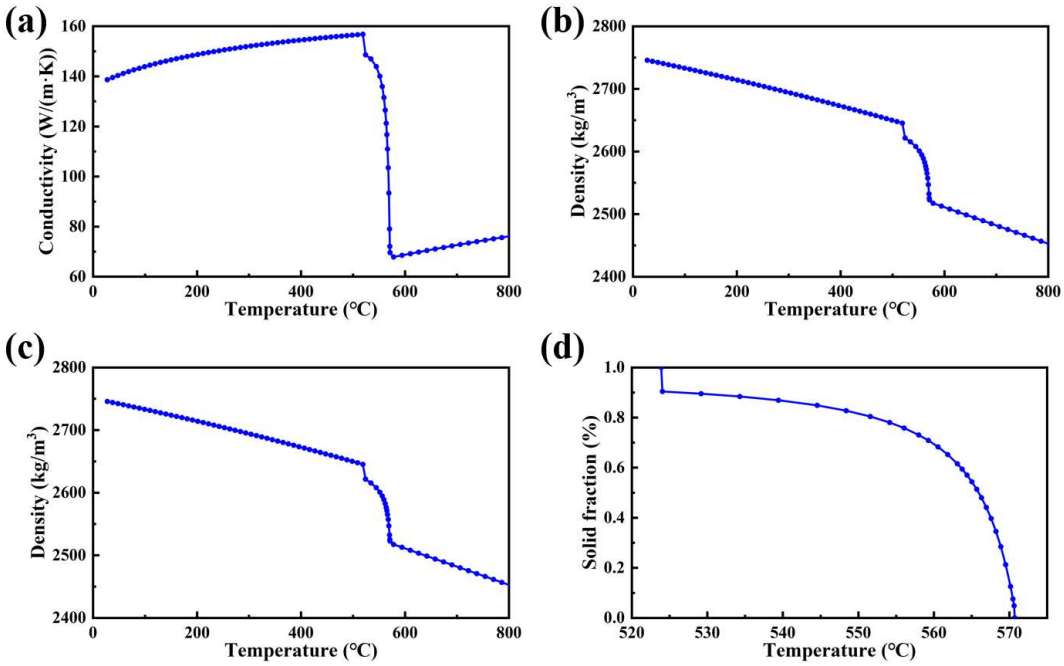


Fig.5 Temperature-dependent properties of ADC12 alloy: (a) thermal conductivity, (b) density, (c) enthalpy, and (d) solid fraction

Table.1 Chemical composition of ADC12 aluminum alloy (wt. %).

element	Si	Cu	Fe	Mn	Mg	Zn
content	9.6-12.0	1.5-3.5	<1.3	<0.5	<0.3	<1.0

According to the experimental parameters, the slow injection stroke of the piston is 225 mm, with a slow injection speed of 0.125 m/s and a fast injection speed of 1.8 m/s. The ambient temperature is set to 30°C, and the initial temperature of the molten alloy is 700°C.The interfacial heat transfer coefficient between the molten alloy and the mold varies dynamically with the liquid fraction at the interface. When the alloy temperature at the mold wall (T_w, °C) is between the solidus and the liquidus, the interfacial heat transfer coefficient (h_i, W/(m²·K)) is as follows.

$$h_i=61.5T_w-30692.3 \ (515°C < T_w < 580°C) \quad (5)$$

The initial mold temperature is an important parameter in die casting simulations. A typical thermal cycle of the HIDC process is shown in Fig.6. After 40 thermal cycles, the initial mold temperature stabilizes and is determined to be 305.5°C, as shown in Fig.7. The flow rate–time curve used in the simulation is derived from experimentally measured pressure–time data through inverse analysis, as illustrated in Fig.8.

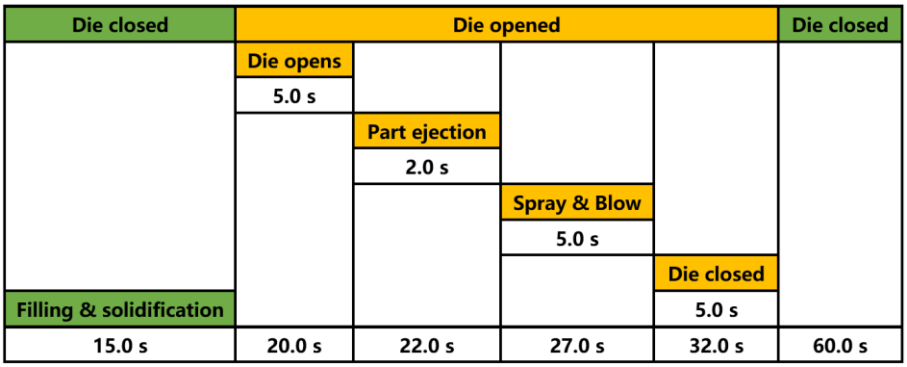


Fig.6 Cycle timing of HIDC

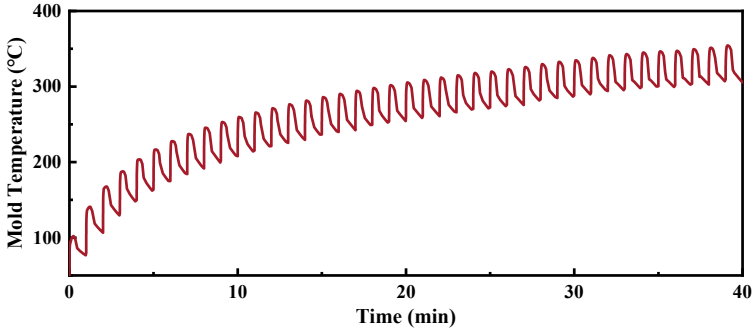


Fig.7 Thermal cycle simulation

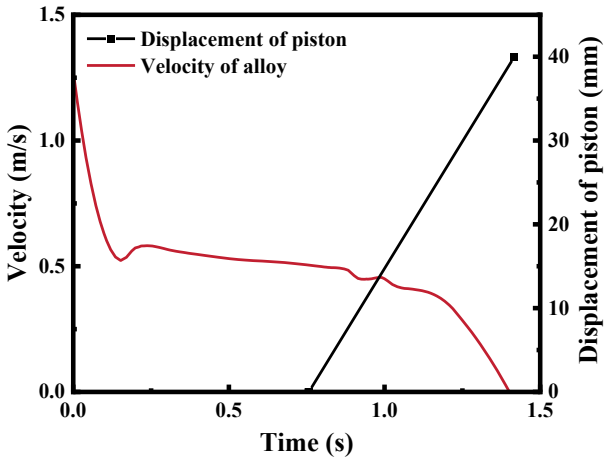


Fig.8 Typical inflow velocity-piston displacement-time curve

3.3 Validation of Simulation Method

A tetrahedral unstructured mesh was generated using the Visual-Mesh module. Five different mesh densities (7.81 million, 11.82 million, 22.95 million, 34.09 million, and 55.04 million elements) were tested (Fig.9b). The results showed that when the number of mesh elements exceeded 34.09 million, further refinement had a negligible effect on the simulation results. Therefore, the model with 34.09 million elements was selected for subsequent simulations. In the selected mesh, the maximum element size

in the casting domain was less than 0.9 mm, while that in the shot sleeve domain was less than 1.8 mm. The mesh size in the mold and shot sleeve solid domains was less than 15 mm, as illustrated in Fig.9a.

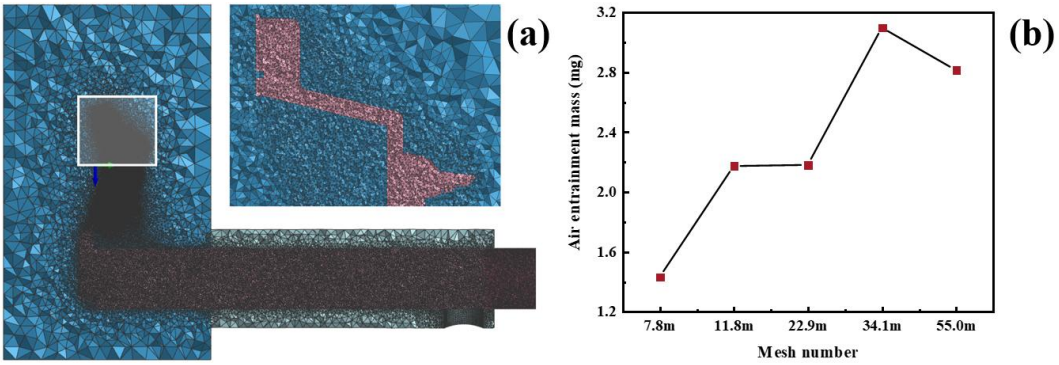


Fig.9 HIDC simulation mesh: (a) Overall schematic of the mesh; (b) Mesh independence verification

To verify the accuracy of the numerical simulation method, the predicted defect distributions were compared with the actual defects observed in the castings. Fig.10 presented a comparison between the simulated total porosity and the experimentally measured porosity area based on X-ray imaging. The absolute error between the simulation results of porosity and the experimental results is at most 3.02% and at least 0.16%. The filling percentage, defined as the proportion of molten alloy occupying the shot sleeve volume, is a unique process parameter in the HIDC system. The results showed that, with increasing filling percentage, the porosity of the casting first decreased rapidly and then increased gradually. The simulation results were in good agreement with the experimental data, indicating that the developed numerical model effectively captured the evolution of porosity under different process conditions. Within the 50% to 90% filling percentage range, the HIDC process yields a porosity level below 1%. Notably, castings produced with a 60% filling percentage possess the smallest equivalent pore diameter of 0.43 mm. Since the equivalent pore diameter is a dominant factor influencing the mechanical properties of die-cast components, a filling percentage of 60% was selected as the typical process for the HIDC process in this study[26].

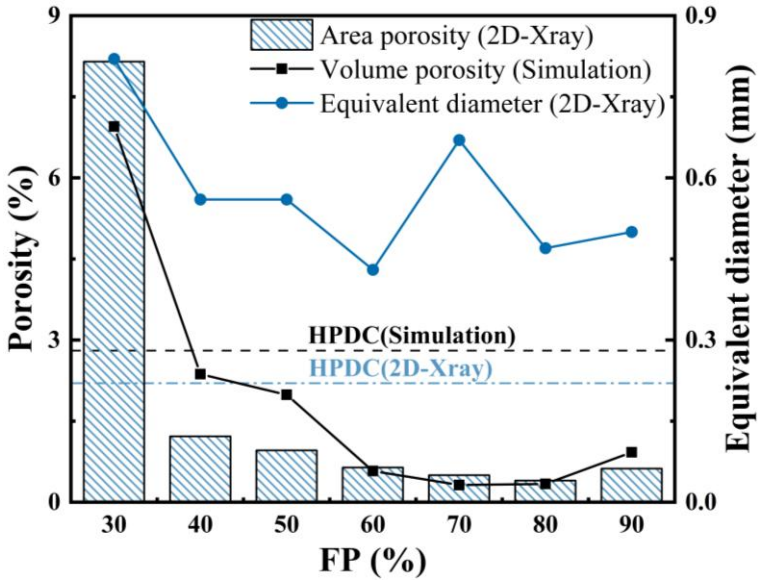


Fig.10 Comparison between experimental and numerical simulation results on porosity

Fig.11 compared the simulated gas entrapment defects with X-ray observations for both conventional HPDC and HIDC-30% conditions. The results showed that gas entrapment defects in both processes were mainly distributed in the central region and upper edge of the casting. For the HIDC-30% condition, more severe and concentrated gas entrapment defects were observed in the central region. The predicted defect distribution agreed well with the experimental observations, demonstrating the reliability of the simulation in predicting gas entrapment behavior.

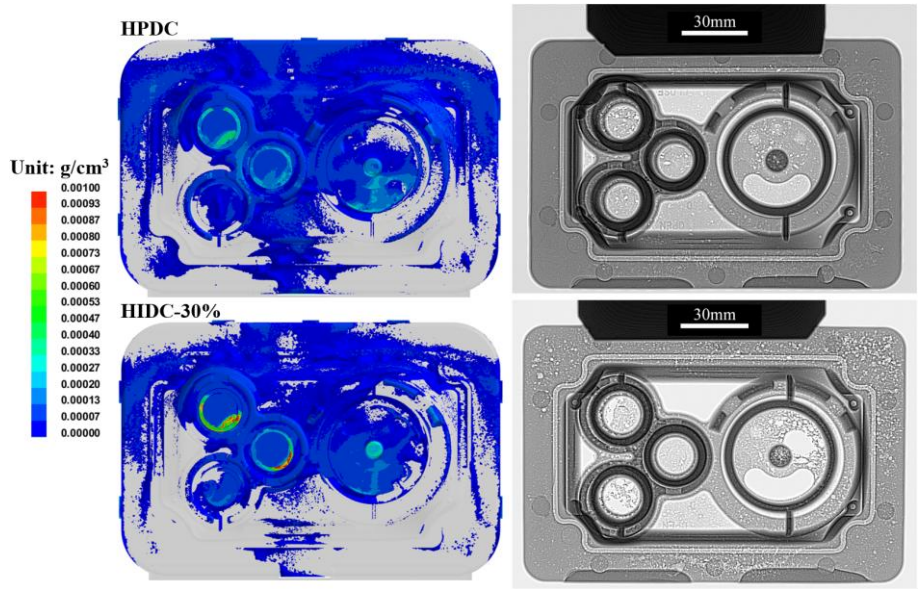


Fig.11 X-ray imaging versus simulation prediction of gas entrapment distribution in the casting

Fig.12 illustrated the stratified solidification defects under the HIDC-90% condition. The simulation results showed that, during mold filling, the molten alloy

exhibited pronounced upward flow followed by fallback. This flow behavior led to the formation of a prematurely solidified thin shell at the top corner regions of the casting. Correspondingly, the experimental castings exhibited stratified solidification defects in these regions, confirming the validity of the simulation prediction.

Overall, the numerical simulation results showed good agreement with experimental observations in terms of defect type, distribution, and evolution trend. It confirmed that the developed model accurately described the flow and heat transfer behavior of the HIDC process and could be reliably used for defect prediction and process analysis.

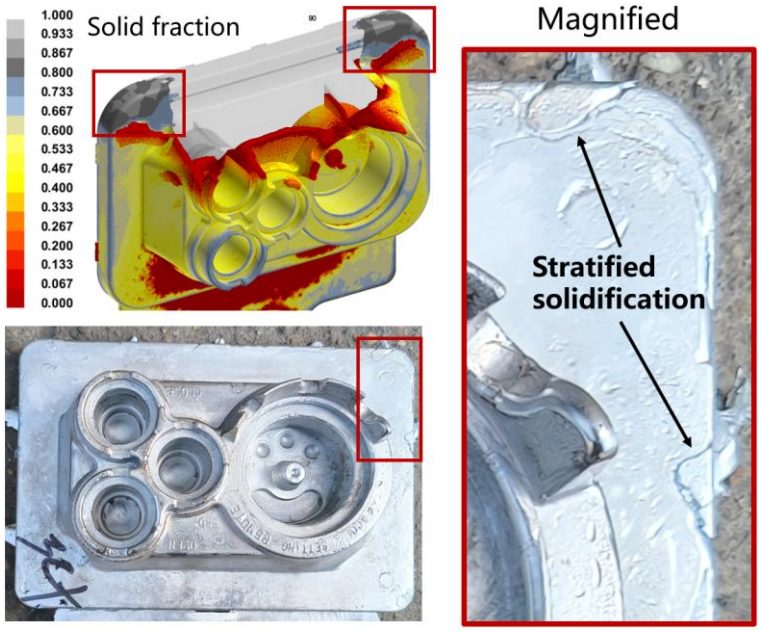


Fig.12 Stratified solidification defect in HIDC-90%

4. Simulation Result

4.1 Typical HIDC Process

(1) Flow field evolution of Typical HIDC Process

In conventional die casting simulations, the dynamic process of molten metal pouring into the shot sleeve is often neglected, and the initial condition is typically simplified as a static, uniform, and isothermal melt. In contrast, the present study captures the complete transient behavior of the molten alloy, including its entry into the shot sleeve, oscillatory flow within the sleeve, and subsequent filling of the mold cavity

under piston-driven injection, thereby providing a more realistic representation of the actual casting process.

Fig.13 shows the transient flow behavior of the molten alloy in the shot sleeve under the HIDC-60% condition. At 0.49 s, the molten alloy flows rightward at approximately 0.7 m/s. At 1.11 s, after impinging on the right wall of the shot sleeve, the melt reverses direction and flows leftward at about 0.4 m/s. Meanwhile, the injection piston continuously pushes the newly introduced melt, generating a counter-propagating flow wave. At 1.66 s, the two opposing flow waves collide, and by 1.71 s, their velocity vectors gradually cancel each other, resulting in dissipation of kinetic energy and stabilization of the melt surface. At 1.91 s, the piston enters the slow injection stage, pushing the molten alloy toward the right. This motion increases the melt level on the left side and drives the residual gas toward the mold cavity. At 2.21 s, the melt front reaches the ingate, with an average velocity of approximately 0.13 m/s.

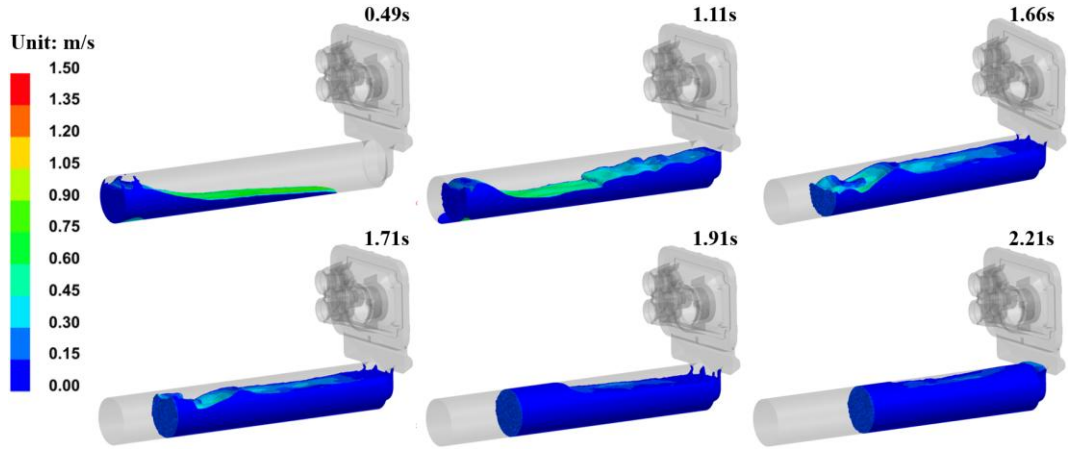


Fig.13 Velocity field in the HIDC-60% shot sleeve

Fig.14 illustrates the mold filling process of the molten alloy in the cavity under the HIDC-60% condition. During the slow injection stage (Fig.14 I), the injection piston pushes the molten alloy into the cavity at a velocity of approximately 0.5 m/s. Subsequently, the melt fills the cavity from bottom to top (Fig.14 II), with flow velocities of about 0.05–0.2 m/s in the edge regions and higher velocities of 0.2–0.4 m/s in the central region. At the stage shown in Fig.14 III, the molten alloy continues to advance steadily at a relatively low velocity, while the liquid levels in the edge and central regions remain nearly uniform, thereby gradually driving the gas within the cavity toward the top exhaust channels. When the piston switches to the fast injection

stage (Fig.14 IV), the flow velocity in the central region increases to 4–6 m/s, while that in the edge regions further rises to 4–10 m/s. At the final stage of filling (Fig.14 V), the central region is filled first due to its shorter flow path, and the molten alloy from the edge regions rapidly converges toward the center. This flow pattern effectively expels most of the remaining gas through the top exhaust ports, thereby significantly suppressing gas entrapment defects.

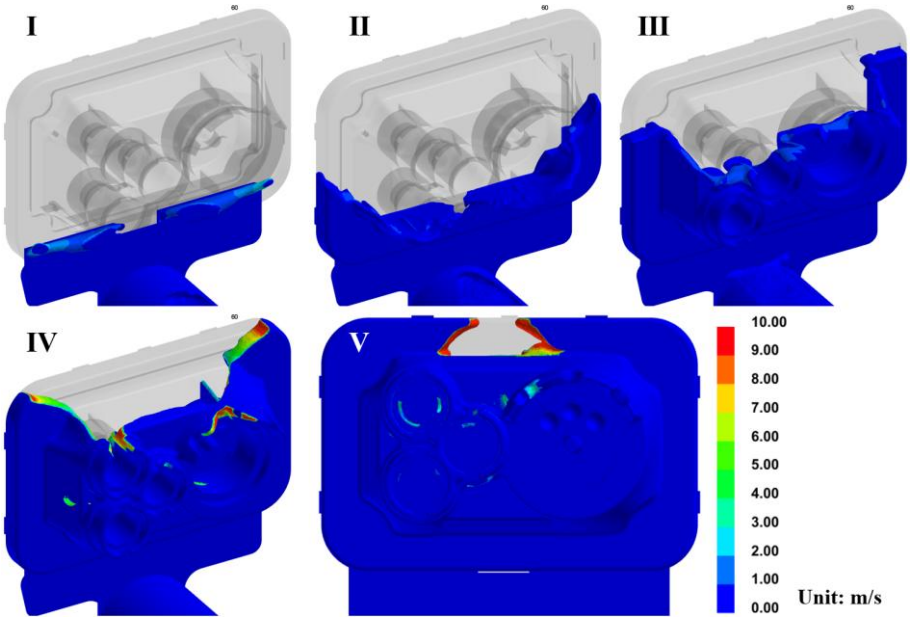


Fig.14 Velocity field in the HIDC-60% die cavity

In the HIDC-60% process, when the molten alloy reached the mold cavity entrance, air remained trapped in the shot sleeve. Fig.15 shows the movement of this trapped air during mold cavity filling. In the initial stage of cavity filling, the molten alloy filled the cavity uniformly in height. The air trapped in the sleeve moved towards the mold cavity due to the density difference (Fig.15a). As the liquid level rose, part of the air separated from the trapped air in the sleeve, forming bubbles that moved upward (Fig.15b). The liquid level continued to rise, with bubbles splitting and gradually floating to the surface of the molten alloy, accompanied by the generation of new bubbles (Fig.15c). At the end of cavity filling, most of the air originally trapped in the sleeve floated out of the molten alloy surface and was expelled through the vents (Fig.15d). For the HIDC-60% process, the air trapped in the sleeve did not cause excessive gas entrapment defects in the casting.

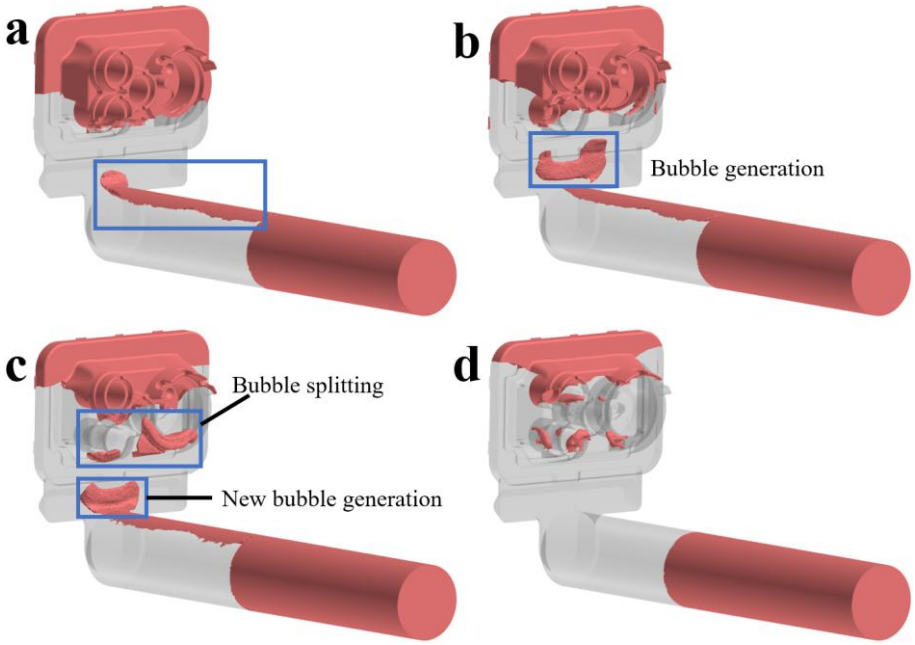


Fig.15 Evolution of trapped air in the shot sleeve during filling under HIDC-60% condition

(2) Temperature field evolution of Typical HIDC Process

During the filling stage, the heat transfer rate at the interface between the molten alloy and the mold is relatively low. The resulting slow cooling conditions promote the formation of coarse grains in the melt. The heat transfer characteristics at this stage directly influence the quantity and size distribution of externally solidified crystals (ESCs) in the casting. During the subsequent solidification stage, under the effect of high injection pressure, the heat transfer intensity between the molten alloy and the mold wall increases significantly, thereby promoting grain refinement. Meanwhile, the temperature gradient and cooling rate at this stage jointly determine the location and severity of shrinkage defects.

During the die casting process, the heat transfer behavior in the flow stage can be divided into two sub-stages: heat transfer during flow in the shot sleeve and heat transfer during flow in the mold cavity. In this study, the initial temperature of the molten alloy is 700 °C. Fig.16a shows the temperature distribution at the end of the shot sleeve flow stage under different processes. In the conventional high-pressure die casting process, the relatively longer filling time results in a longer residence time of the molten alloy in the shot sleeve, leading to significant heat loss and a substantial overall temperature drop. In contrast, the HIDC process features a more compact

process sequence, which effectively shortens the residence time of the molten alloy in the shot sleeve. As a result, the low-temperature regions are less extensive, and the temperature drop during the shot sleeve flow stage is significantly reduced. Since the formation of ESCs is closely related to the cooling rate and undercooling of the molten alloy, the improved temperature retention in the shot sleeve under the HIDC process effectively suppresses premature solidification of the melt, thereby significantly reducing the formation of ESCs[27].

The flow behavior within the mold cavity directly influences the temperature distribution at the end of the filling stage, as shown in Fig.16b. In the conventional high-pressure die casting (HPDC) process, the molten metal at the front of the shot sleeve exhibits a relatively high temperature. Due to the high filling velocity, the heat loss during flow is limited, allowing this high temperature melt to ultimately fill the upper edge and central regions of the casting. As a result, localized hot spots are formed in these regions, which are prone to shrinkage defects due to insufficient feeding during solidification. In contrast, under the HIDC-60% condition, the filling velocity during the mold filling stage is relatively low. The molten alloy at the flow front undergoes significant cooling during filling, resulting in an overall lower temperature in the upper regions of the casting. Consequently, the high-temperature zones are mainly located in the bottom edge regions, where the molten metal enters the cavity later and experiences shorter cooling times.

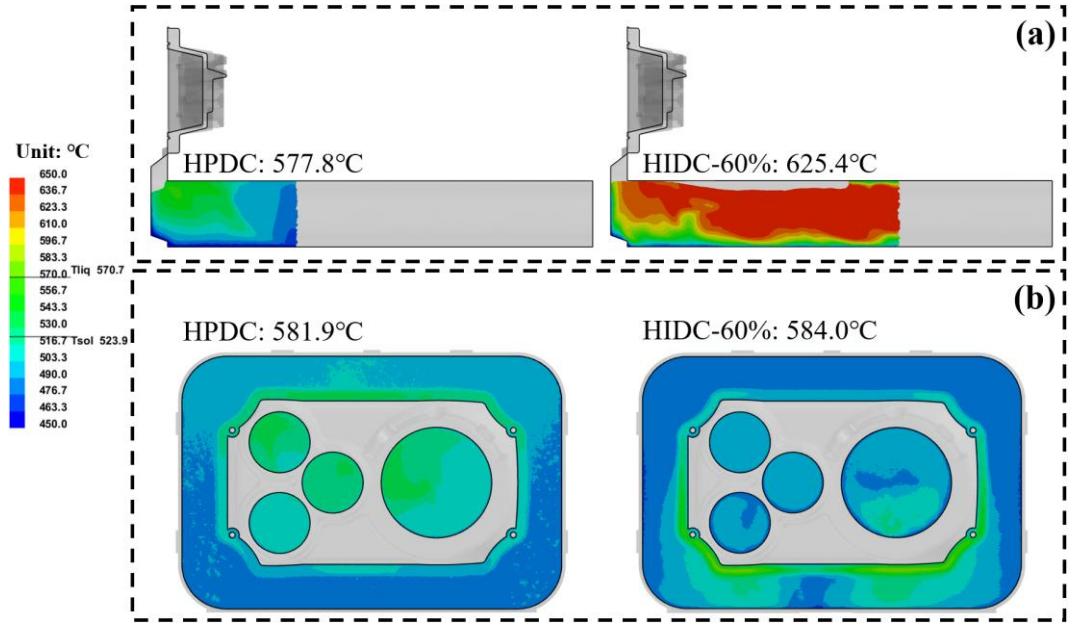


Fig.16 Cross-section temperature fields of die cavity filling: (a)initial stages; (a)final stages

(3) solidification fraction evolution of Typical HIDC Process

The temperature distribution at the end of mold filling directly affects the evolution of the temperature field during the subsequent solidification process. Fig.17 presents the solidification behavior of the casting under conventional HPDC and HIDC-60% conditions. Due to the relatively lower filling velocity and longer flow path in the HIDC-60% process, the upper edge regions exhibit a relatively high solid fraction at the end of filling, while the remaining regions maintain a lower solid fraction. As a result, the solidification process of the casting under the HIDC-60% condition generally follows a sequence in which regions farther from the ingate solidify first, followed by regions closer to the ingate. This sequence facilitates continuous feeding of the solidifying regions through the ingate, thereby effectively reducing the overall severity of shrinkage defects in the casting[28].

Fig.18 quantitatively demonstrates the impact of the process on the solidification sequence at different points on the casting, with specific data points shown in Fig.17 (Top: z=47.1mm, Middle: z=0mm, Bottom: z=-47.1mm). For the HPDC process, the solid fraction at the bottom point at the moment of filling completion is 0.36, while the solid fraction at other points of the casting is 0. At 1.92 seconds, the solid fractions at both the bottom and top points reach 0.7, with the middle point remaining at 0, and the thin-walled regions unable to be fed, resulting in shrinkage porosity. For the HIDC-60%

process, the solid fraction at the top point at the moment of filling completion is 0.4, with other points having a solid fraction of 0. The solid fraction at the top point reaches 0.7 in 0.5 seconds, while the solid fraction at the bottom point reaches 0.7 in 1.08 seconds, showing a clear sequential solidification from far to near. At this moment, the solid fraction at the middle point is 0.3, and partial compensation for shrinkage occurs in the thin-walled areas.

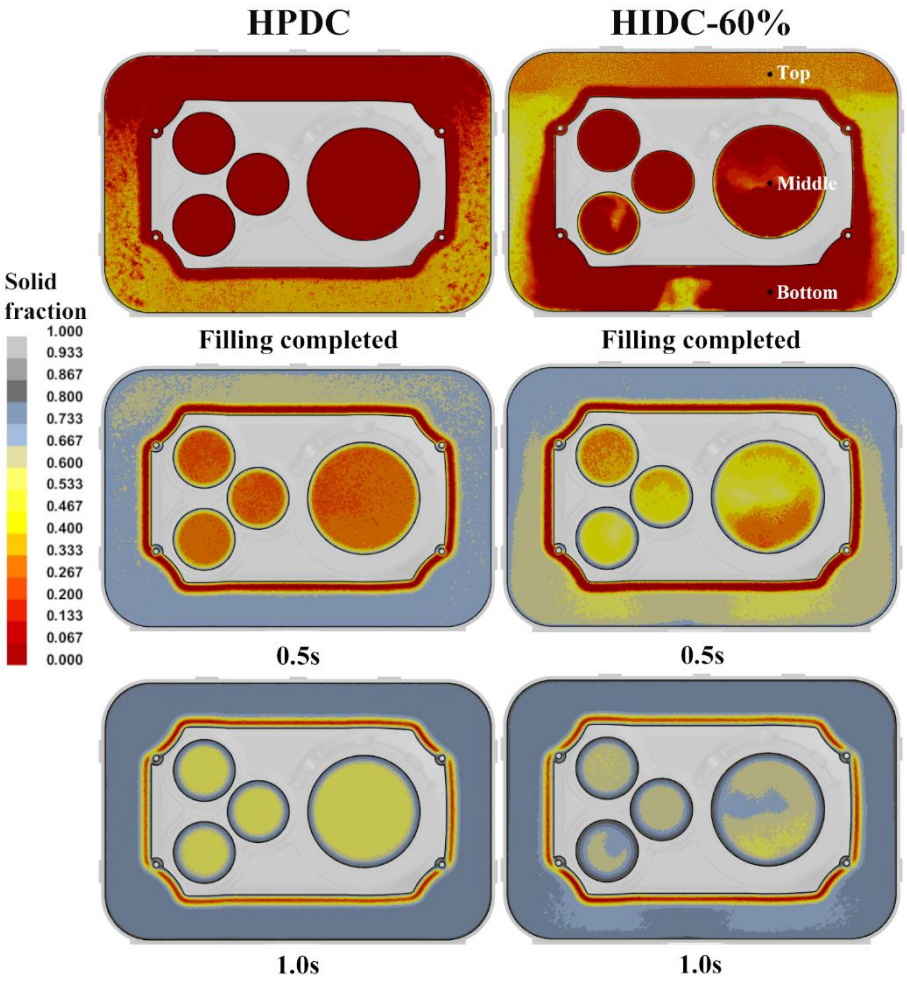


Fig.17 Cross-section distribution and evolution of solid fraction in the die cavity under different processes

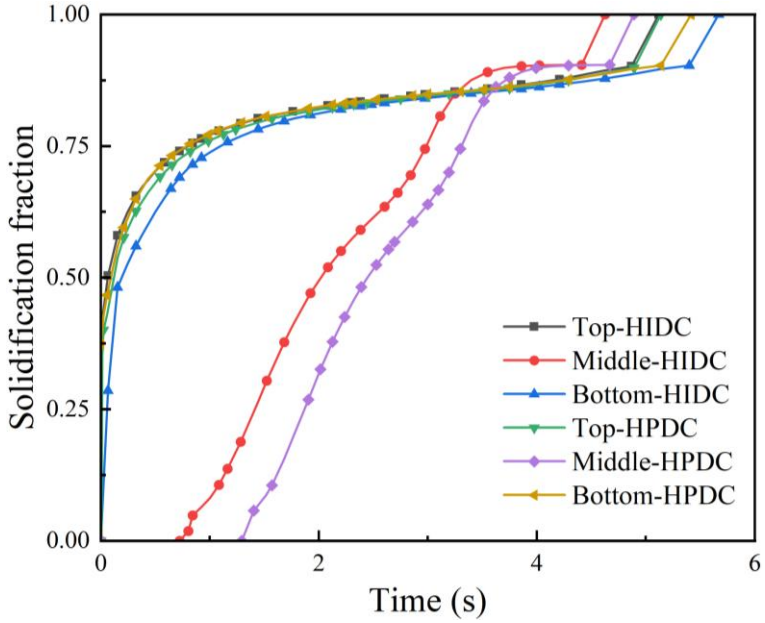


Fig.18 The effect of manufacturing processes on solidification at various points

4.2 Effect of Filling Percentage

The filling percentage is a unique process parameter in the HIDC process. Experimental results indicate that it directly determines the severity of gas entrapment defects in the casting. For the casting investigated in this study, a filling percentage of 60% represents the optimal process window. A lower filling percentage leads to severe porosity defects, whereas a higher filling percentage results in a small number of larger pores as well as stratified solidification defects.

The shot sleeve filling stage under the HIDC-30% condition is shown in Fig.19. At 0.4 s, the low-pressure filling process is not yet completed, and the upward velocity of the molten alloy is redirected into a rightward velocity due to the influence of the wall, resulting in a rightward flow at approximately 0.7 m/s, while the piston moves slowly to the right. At 1.17 s, the molten alloy is concentrated on the right side of the shot sleeve. After impinging on the wall, it reverses direction and flows leftward at about 0.4 m/s, with a reduced velocity. At 1.90 s, as the piston has already moved a certain distance to the right, the melt generates a stronger rightward wave after wall impingement. At 2.13 s, a small portion of the molten alloy enters the mold cavity due to inertia. At 2.31 s, part of the molten alloy that has entered the cavity solidifies on the inner surface, while most of it falls back into the shot sleeve. The piston then enters the fast injection stage, rapidly pushing the molten alloy rightward, increasing the melt

level on the left side and forcing the air in the shot sleeve into the mold cavity. At 2.32 s, the air in the shot sleeve is completely pushed into the mold cavity, and the molten alloy is about to enter the cavity, marking the end of the shot sleeve filling stage. At this moment, the average velocity of the molten alloy in the shot sleeve is approximately 1.69 m/s.

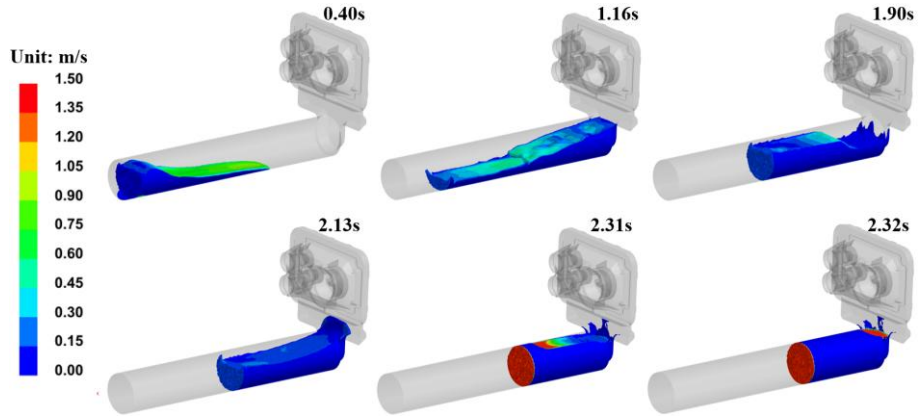


Fig.19 Velocity field in the HIDC-30% shot sleeve

The shot sleeve filling stage under the HIDC-90% condition is shown in Fig.20. At 0.51 s, the molten alloy flows rightward at approximately 0.7 m/s. At 1.00 s, after impinging on the wall, the melt reverses and flows leftward at about 0.5 m/s, while additional molten alloy continues to enter the shot sleeve from the inlet. At 1.54 s, more molten alloy impinges on the wall and moves leftward. At 1.71 s, the leftward-moving molten alloy forms a pronounced wave, resulting in part of the gas being trapped on the left side of the shot sleeve and unable to be discharged. At 1.86 s, the piston slowly pushes the molten alloy rightward. At 1.91 s, the piston drives the mixture of molten alloy and entrapped air, pushing the molten alloy on the right side toward the entrance of the mold cavity. Due to the highest filling percentage in the HIDC-90% process, the molten alloy obtains the greatest momentum from the inlet. At this stage, the average velocity of the molten alloy in the shot sleeve is approximately 0.21 m/s, which is higher than that under the HIDC-60% condition.

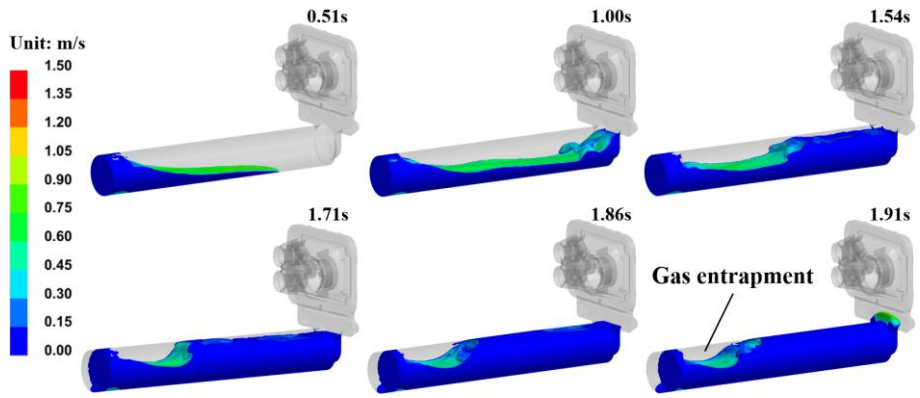


Fig.20 Velocity field in the HIDC-90% shot sleeve

At this stage, all processes enter the mold filling stage. Fig.21 shows the mold filling process under the HIDC-30% condition. As shown in Fig.21 I, the piston has already entered the fast injection stage, and the molten alloy enters the mold cavity at a velocity of approximately 6–7 m/s. As shown in Fig.21 II, the molten alloy fills the cavity from bottom to top. Due to the narrow flow channels and complex geometry in the thin-walled regions, the flow resistance is relatively high. As a result, the flow velocity reaches about 10 m/s in the edge regions, while it is approximately 4–5 m/s in the thin-walled regions. As shown in Fig.21 III–IV, the molten alloy in the edge regions converges first at the upper part of the cavity, blocking the exhaust ports, and then flows downward into the thin-walled regions. As shown in Fig.21 V, the molten alloy pushes the remaining gas in the cavity toward the thin-walled regions, where most of the gas is eventually entrapped in the four circular thin-walled sections.

This flow pattern traps the gas within the casting and ultimately leads to significant gas entrapment defects in the thin-walled regions.

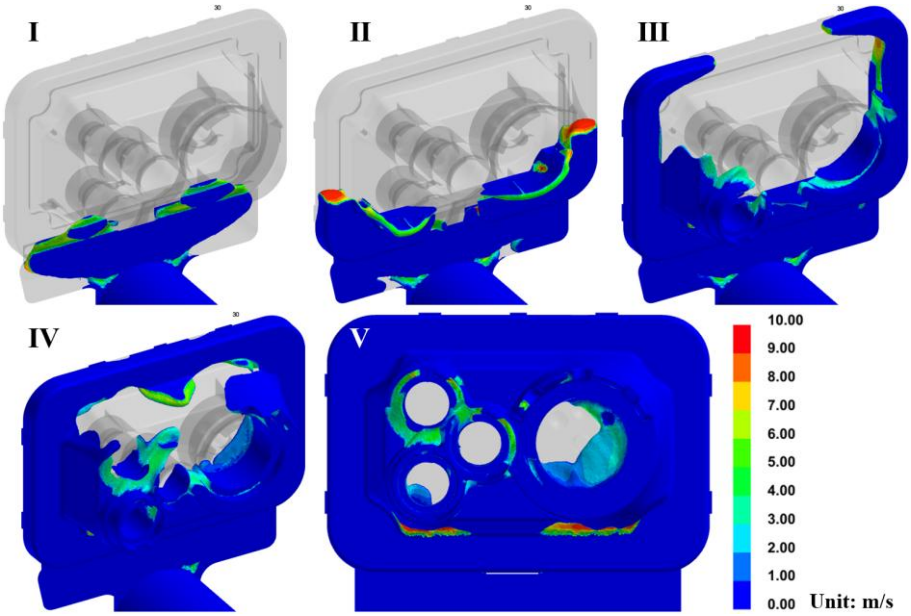


Fig.21 Velocity field in the HIDC-30% die cavity

Fig.22 shows the mold filling process under the HIDC-90% condition. Compared with the HIDC-60% process, the HIDC-90% process exhibits a higher melt velocity at the end of the shot sleeve filling stage. As shown in Fig.22 I, although the piston speed remains the same, the molten alloy enters the mold cavity at a velocity of approximately 0.8–1.6 m/s under the FP = 90% condition. As shown in Fig.22 II, the molten alloy exhibits a filling pattern similar to that of the HIDC-30% process, preferentially filling the edge regions. As shown in Figs.22 III–IV, the molten alloy in the edge regions is driven by inertia toward the corner regions. After the kinetic energy is dissipated, part of the melt falls under gravity, while another portion rapidly loses heat and solidifies at the corners, resulting in stratified solidification defects. As shown in Fig.22 V, under the slow pushing of the piston, the molten alloy fills the mold cavity from bottom to top with low turbulence, and the remaining gas is discharged through the upper exhaust ports.

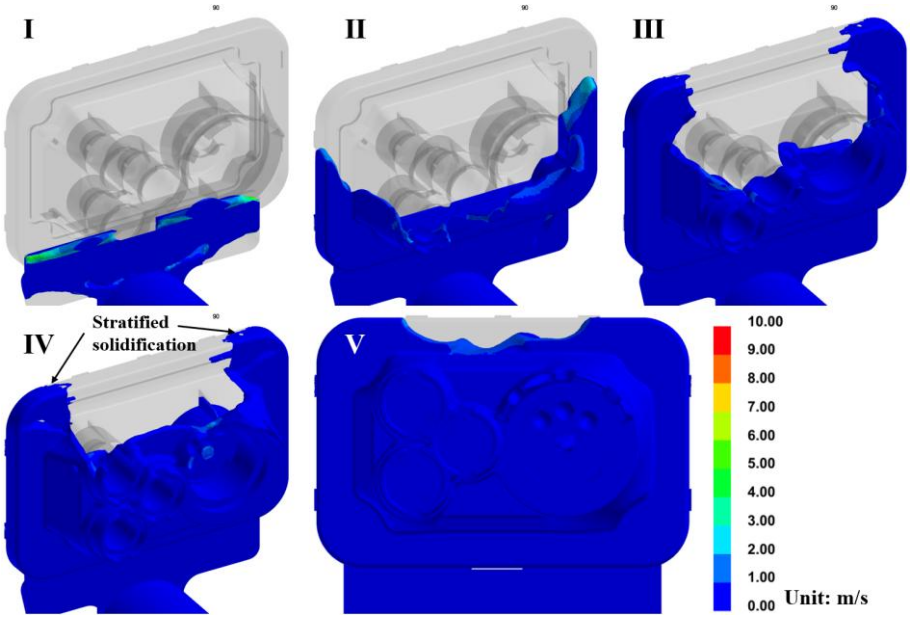


Fig.22 Velocity field in the HIDC-90% die cavity

Gas entrapment occurs during the shot sleeve filling stage under the HIDC-90% condition, and its evolution over time is shown in Fig.23. At the beginning of the mold filling stage, the entrapped gas is located at the rear of the shot sleeve. As the piston pushes the molten alloy into the mold cavity, the entrapped gas moves forward and gradually becomes more elongated in shape, but it does not enter the mold cavity. Eventually, the entrapped gas is compressed into the upper region of the shot sleeve. As a result, severe gas entrapment occurs in the biscuit region, while the gas trapped in the shot sleeve has no significant effect on the quality of the casting.

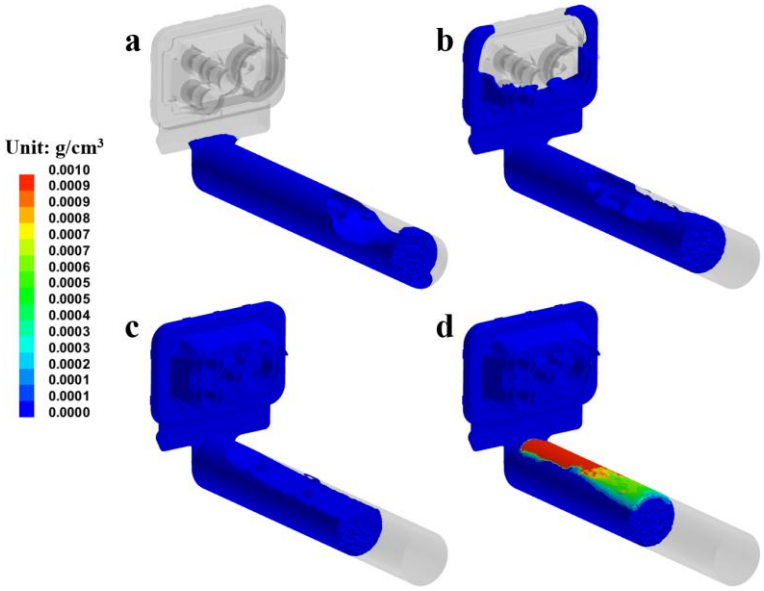


Fig.23 Evolution of trapped gas position under HIDC-90% condition

4.3 Effect of Slow Injection Speed

As demonstrated in the previous section, the slow injection stage has a significant influence on the flow behavior of the molten alloy in the mold cavity. The flow pattern within the cavity is a major source of gas entrapment defects. Therefore, this section investigates the effect of slow injection speed on the HIDC casting process. In this study, three slow injection speeds—0.09 m/s, 0.125 m/s (typical condition), and 0.16 m/s—are examined under a filling percentage of 60%.

The shot sleeve filling stage of the HIDC-60% process with a slow injection speed of 0.09 m/s is shown in Fig.24. Before 2.10 s, the filling behavior is similar to that of the typical process, characterized by “slow filling followed by backflow after wall impingement.” At 2.10 s, the molten alloy impinges on the wall for the second time, generating a rightward-propagating wave with a velocity of approximately 0.2 m/s, which is significantly higher than the piston velocity. At 2.40 s, this wave reaches the entrance of the flow channel. At 2.93 s, a small amount of molten alloy enters the mold cavity under the inertia of the wave and subsequently falls back under the action of gravity. This phenomenon leads to the formation of stratified solidification defects in the lower region of the casting.

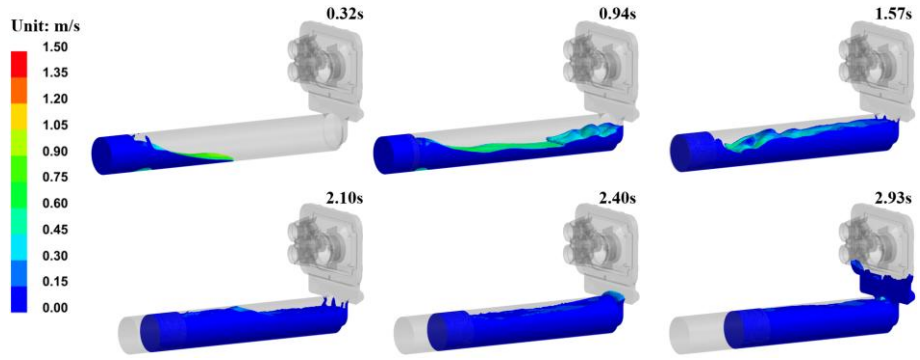


Fig.24 Velocity contours of shot sleeve filling under HIDC-60% condition at a slow injection speed of 0.09 m/s

The shot sleeve filling stage of the HIDC-60% process with a slow injection speed of 0.16 m/s is shown in Fig.25. Before 1.86 s, the molten alloy exhibits a flow pattern characterized by “slow filling followed by backflow after wall impingement.” At 1.86 s, the piston pushes the molten alloy rightward at a relatively higher velocity. At 2.08 s, the molten alloy reaches the entrance of the flow channel. Because the piston velocity

at a slow injection speed of 0.16 m/s is comparable to the rightward wave velocity generated during filling, the molten alloy does not enter the mold cavity prematurely due to inertia. As a result, stratified solidification defects are effectively avoided in the casting.

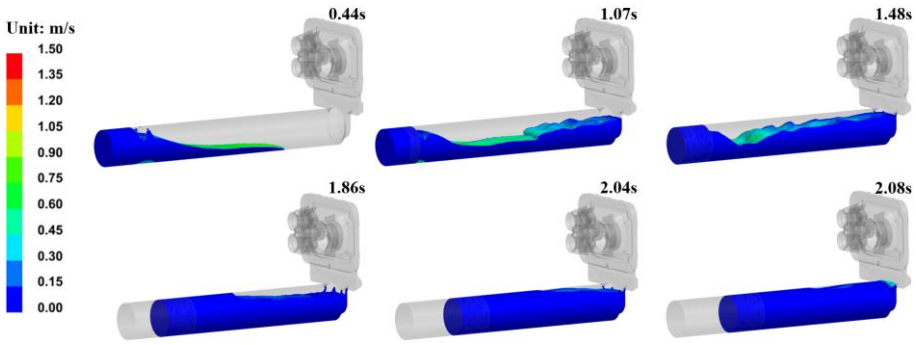


Fig.25 Velocity contours of shot sleeve filling under HIDC-60% condition at a slow injection speed of 0.16 m/s

Fig.26 shows the mold filling process of the HIDC-60% condition with a slow injection speed of 0.09 m/s. As shown in Fig.26 I–II, the molten alloy enters the mold cavity under inertia and subsequently falls back under the action of gravity, leaving a stratified solidified shell on the lower surface of the casting. As shown in Fig.26 III, due to the lowest slow injection speed, the molten alloy fills the cavity from bottom to top in a more horizontal and stable manner, resulting in the least gas entrapment defects. As shown in Fig.26 IV–V, the molten alloy in the edge regions rapidly converges toward the center, expelling most of the gas through the exhaust ports. This filling pattern effectively suppresses gas entrapment defects; however, the influence of stratified solidification defects on the mechanical properties of the casting cannot be neglected.

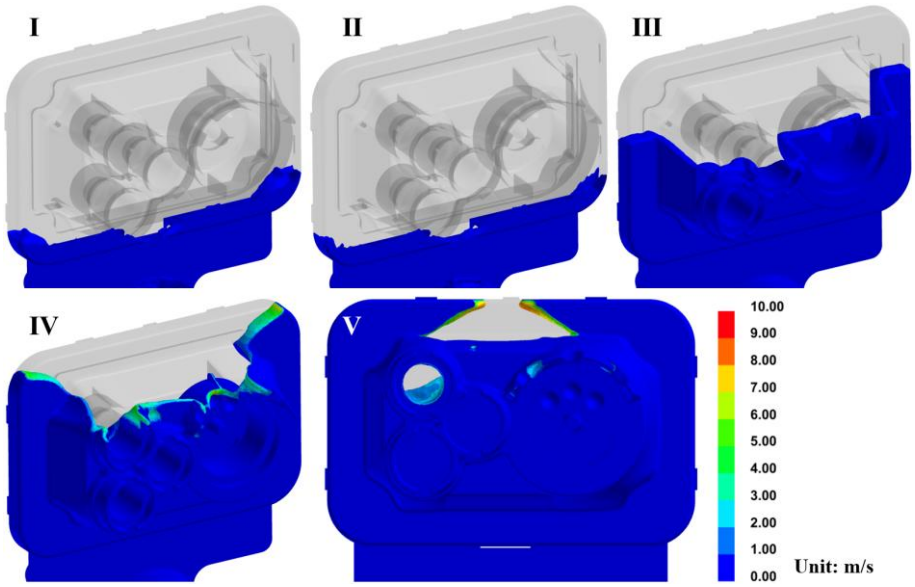


Fig.26 Velocity contours of die cavity filling under HIDC-60% condition at a slow injection speed of 0.09 m/s

Fig.27 shows the mold filling process of the HIDC-60% condition with a slow injection speed of 0.16 m/s. As shown in Fig.27 I–II, the molten alloy enters the mold cavity at a velocity of approximately 0.7 m/s and preferentially fills the edge regions of the cavity. As shown in Fig.27 III, the melt maintains a nearly uniform liquid level and fills the cavity from bottom to top. As shown in Figs.27 IV–V, the molten alloy in the edge regions rapidly converges toward the center, expelling most of the gas through the exhaust ports.

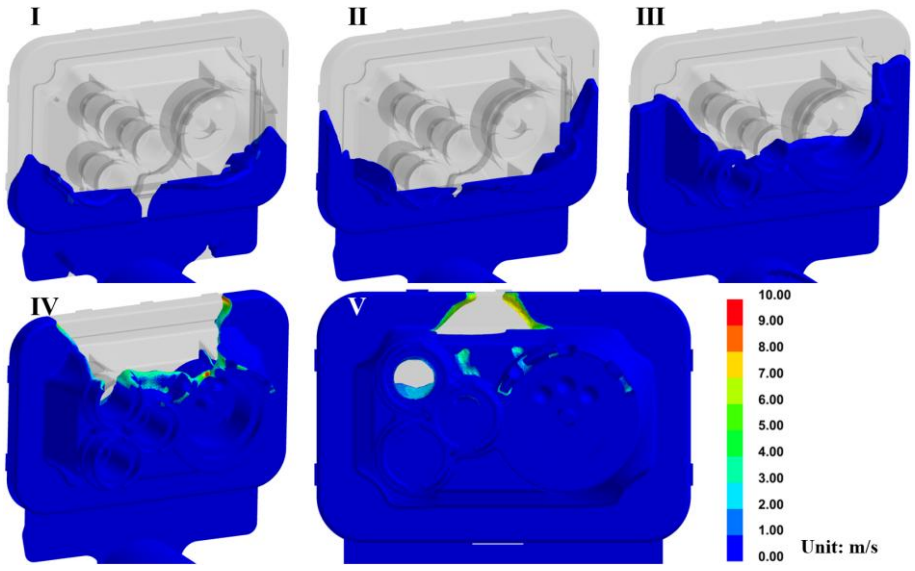


Fig.27 Velocity contours of die cavity filling under HIDC-60% condition at a slow injection speed of 0.16 m/s

The effect of slow injection speed on the air entrainment process in the mold cavity is shown in Fig.29, with the moment of alloy melt entering the cavity being at time 0 in the figure. For the HIDC process with a slow injection speed of 0.09 m/s, the gas volume fraction reaches its maximum value of 28.5% at 0.54 seconds (3.1 seconds into the entire process) during mold filling. At this time, the filling pattern of the molten alloy corresponds to the "upward surge - fallback" mode (Figure 26, I-II). Subsequently, the gas content in the injection cylinder decreases as the following metal melt continues to fill the mold cavity, reducing the overall gas entrainment. The final porosity of the casting is 7.2%.

The simulation results indicate that, under a filling percentage of 60% and slow injection speeds of 0.09 m/s, 0.125 m/s, and 0.16 m/s, the volumetric gas entrapment of the castings is 7.2%, 0.45%, and 0.29%, respectively. A higher slow injection speed results in a lower gas entrapment ratio. Fig.28 shows the gas entrapment behavior during the filling process of the HIDC-60% condition with a slow injection speed of 0.09 m/s. It can be observed that the primary gas entrapment occurs between 2.93 s and 3.13 s. During this period, the molten alloy surges upward and subsequently falls back. This small-scale “backflow” phenomenon significantly increases the gas entrapment ratio, ultimately leading to pores remaining within the casting.

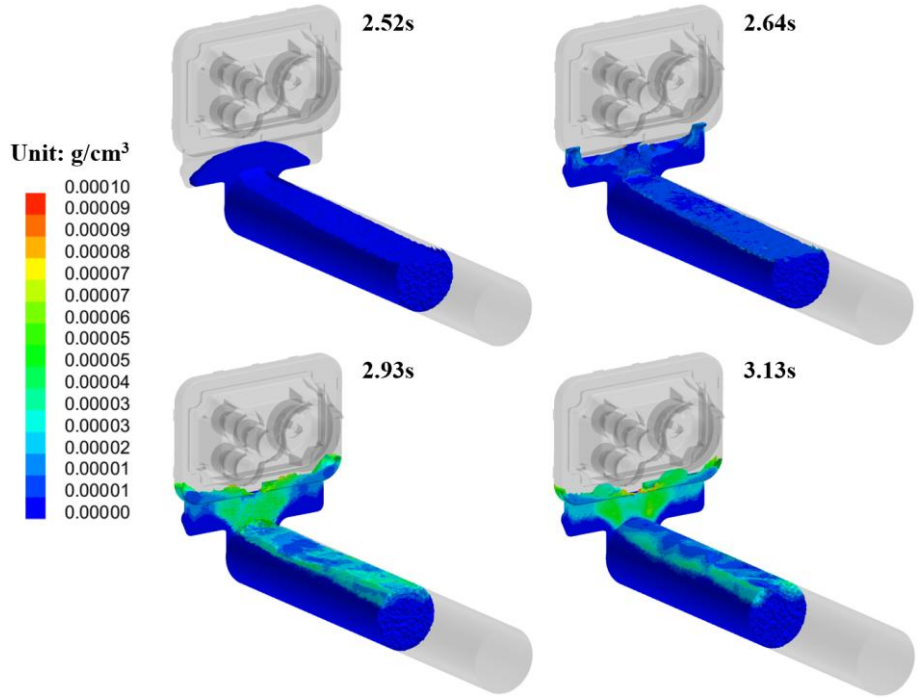


Fig.28 Gas entrapment distribution during filling under HIDC-60% condition at a slow injection speed of 0.09 m/s

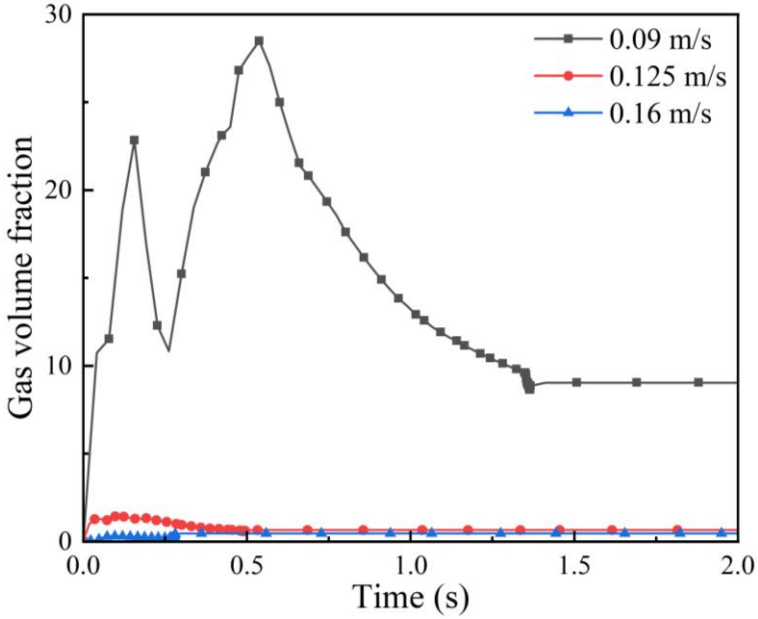


Fig.29 The effect of slow injection speed on the gas entrapment process

5. Conclusion

This study systematically investigates the forming mechanisms and defect control characteristics of the highly integrated die casting (HIDC) process through comprehensive numerical simulations. The main conclusions are summarized as follows:

The numerical simulation model established in this study accurately reproduces the complete HIDC process. The absolute error between the simulation results of porosity and the experimental results is at most 3.02% and at least 0.16%. The filling percentage is identified as the primary factor determining the type and severity of defects. Both simulations and experimental results indicate that castings produced with a 60% filling percentage exhibit the smallest equivalent pore diameter (0.43 mm), establishing this condition as the typical process.

The typical process of HIDC has the following characteristics. During the shot sleeve filling, the superheat loss for HIDC is only 74.6°C, which is substantially lower than the 122.2°C observed in the HPDC process. During the mold cavity filling, the melt front propagates steadily, thereby facilitating gas expulsion. During the solidification, the solid fraction in the distal region reaches 0.7 at 0.5 s, while that in the

proximal region near the gate attains 0.7 at 1.08 s, indicating an ordered solidification sequence. As a result, both shrinkage and gas entrapment defects are comprehensively reduced.

The slow injection speed directly influences the initial flow behavior in the mold cavity. The simulation results indicate that increasing the slow injection speed (from 0.09 m/s to 0.16 m/s) reduces gas entrapment caused by melt backflow. As the slow injection speed increases from 0.09 m/s to 0.16 m/s, the casting porosity decreases from 7.2% to 0.29%.

This study clearly reveals, through numerical simulation, the oscillatory flow of the molten alloy in the shot sleeve, the processes of gas entrapment and evacuation, as well as the filling sequence and temperature field evolution within the mold cavity—details that are difficult to capture experimentally. The simulation results provide an efficient analytical tool for understanding the fundamental mechanisms of the HIDC process, predicting defects, and precisely optimizing process parameters.

Funding

The research leading to these results received funding from National Key Research and Development Program of China under Grant Agreement No. 2016YFB0301001.

Reference

[1] L. Gozali, K.V. Liu, A. Adianto, S.R. Nasution, C.O. Doaly, Case. Studies. Chem. Environ. Eng, 13 (2026) https://doi.org/10.1016/j.cscee.2025.101315.
[2] A. Celik, A.A. Alola, Energy, 312 (2024) https://doi.org/10.1016/j.energy.2024.133520.
[3] J. Qi, D.C. Dunand, Acta. Mater, 282 (2025) https://doi.org/10.1016/j.actamat.2024.120452.
[4] R. Peng, H. Liu, P. Yi, M. Ao, J. Alloys Compd, 1010 (2025) https://doi.org/10.1016/j.jallcom.2024.177159.
[5] D. Blondheim, A. Monroe, Int. J. Metalcast, 16 (2022) 10.1007/s40962-021-00602-x.
[6] M. Huang, J. Jiang, Y. Wang, T. Qin, X. Zhang, J. Dong, J. Cui, L. Kong, C. Wang, J. Mater. Sci. Technol, 36 (2025) 10.1016/j.jmrt.2025.03.198.
[7] H. Cao, M. Hao, C. Shen, P. Liang, Vac, 146 (2017) https://doi.org/10.1016/j.vacuum.2017.09.048.

[8] X. Dong, X. Zhu, S. Ji, J. Mater. Process. Technol, 266 (2019) https://doi.org/10.1016/j.jmatprotec.2018.10.030.
[9] W. Wen, A.A. Luo, T. Zhai, Y. Jin, Y.-T. Cheng, I. Hoffmann, Scr. Mater, 67 (2012) https://doi.org/10.1016/j.scriptamat.2012.08.010.
[10] J. Yang, B. Liu, D. Shu, H. Li, Q. Yang, T. Hu, Z. Wang, Y. Zeng, J. Huang, X. Tang, J. Alloys Compd, 1026 (2025) https://doi.org/10.1016/j.jallcom.2025.180531.
[11] A. Narimannezhad, H. Aashuri, A.H. Kokabi, A. Khosravani, J. Mater. Process. Technol, 209 (2009) https://doi.org/10.1016/j.jmatprotec.2008.10.004.
[12] K. Natori, H. Utsunomiya, T. Tanaka, J. Mater. Process. Technol, 297 (2021) https://doi.org/10.1016/j.jmatprotec.2021.117277.
[13] S.K. Gautam, B.K. Singh, R.K. Singh, S.K. Tiwari, R. Upadhyaya, H. Khandelwal, G. Kumar, S.M.M. Hasnain, R. Zairov, Results in Engineering, 25 (2025) https://doi.org/10.1016/j.rineng.2025.104453.
[14] A.A. Luo, A.K. Sachdev, D. Apelian, J. Mater. Process. Technol, 306 (2022) https://doi.org/10.1016/j.jmatprotec.2022.117606.
[15] W. Bai, Q. Xu, Z. Han, B. Chen, H. Zhao, Mater. Sci. Eng. A, 943 (2025) 10.1016/j.msea.2025.148742.
[16] J. Zheng, X. Hu, Y. Fu, K. Zhou, W. Sun, Y. Wang, D. Jia, Y. Fu, D. Sun, Wear, 595 (2026) https://doi.org/10.1016/j.wear.2026.206580.
[17] S.K. Gautam, H. Roy, A.K. Lohar, S.K. Samanta, Int. J. Metalcast, 17 (2023) 10.1007/s40962-023-00958-2.
[18] R. Arcaleni, A. Mantelli, L. Girelli, L. Tonelli, A. Morri, A. Pola, L. Ceschini, Mater. Charac, 220 (2025) https://doi.org/10.1016/j.matchar.2024.114657.
[19] P. Dudek, J. Białoń, J. Piwowońska, W. Walczak, K. Wrzała, Vac, 210 (2023) 10.1016/j.vacuum.2023.111859.
[20] N. Balasubramani, A. Ktari, M. El Mansori, Materialia, 42 (2025) https://doi.org/10.1016/j.mtla.2025.102479.
[21] J. Dong, J. Jiang, Y. Wang, T. Qin, M. Huang, J. Cui, X. Zhang, L. Kong, J. Chen, Results in Engineering, 26 (2025) https://doi.org/10.1016/j.rineng.2025.105399.
[22] M.G. Mahmoud, A. Abdelghany, S. Salem, Int. J. Metalcast, 17 (2022) 10.1007/s40962-022-00797-7.
[23] K. Dou, E. Lordan, Y.J. Zhang, A. Jacot, Z.Y. Fan, IOP conference series. Materials Science and Engineering, 529 (2019) 10.1088/1757-899X/529/1/012058.
[24] T. Wang, J. Huang, H. Fu, K. Yu, S. Yao, Applied sciences, 12 (2022) 10.3390/app12094757.
[25] Z. Chen, Y. Li, F. Zhao, S. Li, J. Zhang, Measurement and control (London), 55 (2022) 10.1177/00202940221102656.
[26] H.-j. Kang, H.-s. Jang, S.-h. Oh, P.-h. Yoon, G.-h. Lee, J.-y. Park, E.-s. Kim, Y.-s. Choi, Vac, 193 (2021) https://doi.org/10.1016/j.vacuum.2021.110536.
[27] W. Yu, H. Zhan, C.M. Gourlay, Metall. Mater. Trans. A, 55 (2024) 10.1007/s11661-024-07376-x.
[28] A. Schilling, K. Salscheider, H. Rusche, H. Jasak, M. Fehlbier, S. Kohlstädt, Simulation Modelling Practice and Theory, 107 (2021) https://doi.org/10.1016/j.simpat.2020.102231.